



1 **Climatic characteristics of the Jianghuai cyclone and its linkage with**
2 **precipitation during the Meiyu period from 1961 to 2020**

3 Ran Zhu¹, Lei Chen^{1,2}

4 ¹Department of Atmospheric Science, School of Environmental Studies, China University of
5 Geosciences, Wuhan, 430074, China

6 ²Centre for Severe Weather and Climate and Hydro-Geological Hazards, Wuhan, 430074, China

7 Correspondence to: Lei Chen (leichen@cug.edu.cn)

8 **Abstract.** This study examines the climatic characteristics of 202 Jianghuai cyclones
9 and their linkage with precipitation during the Meiyu period from 1961 to 2020. The
10 results show that cyclones mainly originate from eastern Hubei Province and south-
11 central Anhui Province. The frequency of Jianghuai cyclone occurrences shows an
12 increasing trend in 1965-1970, 1990-2000, and after 2020. A decreasing trend is
13 observed for 1970-1990 and 2000-2010. There is a positive correlation coefficient of
14 0.769 between the frequency of cyclone activity and precipitation in the Meiyu period.
15 The percentage of precipitation affected by cyclone activities can reach up to 47%. The
16 anomalous increase in precipitation caused by cyclones above 27°N can reach a
17 maximum of 7 mm/day. In contrast, precipitation is decreased in southern China
18 because of the strengthening positive geopotential height in the Western Pacific
19 subtropical high (WPSH). Precursor negative geopotential height anomalies for these
20 cyclones emerge over the Mongolian region. The abnormal signal of the negative
21 geopotential height can be traced to day -4 at the 500 hPa level. The WPSH and
22 southwest jet are the dominant factors causing abnormal precipitation during Jianghuai
23 cyclones. The significant water vapor convergence anomalies in the middle and lower
24 reaches of the Yangtze River and the southwestward water vapor transport anomalies
25 provide sufficient water vapor for cyclone development.



26 **1. Introduction**

27 The Meiyu front is one of the important weather systems affecting summer
28 precipitation in the middle and lower reaches of the Yangtze River (Pang et al., 2013;
29 Wang et al., 2014; Zhou et al., 2022; Tao et al., 1979). From mid-June to early July, the
30 east of Yichang, Hubei Province, has continuous rains and short sunshine. These
31 conditions are accompanied by heavy rainfall, strong wind and other weather
32 phenomena in these areas during the Meiyu period (Ding, 1992,1994; Zhao et al., 2021;
33 Zhou et al., 2016). In China, the mean annual precipitation during the Meiyu period in
34 the Jianghuai River Basin can reach 300 mm, accounting for 30%-40% of the mean
35 annual total precipitation, and even up to 500 mm or more in the extreme Meiyu period
36 (Liu et al., 2020). Historically, most of the summer flood disasters are caused by
37 precipitation anomalies in the Meiyu period. Some scholars have studied and analyzed
38 the representative floods of 1996, 1998, 2016 and 2020 (Bao et al., 2021; Su et al., 2021;
39 Zhao et al., 2018; Zhong et al., 2023). These floods, caused by the Meiyu front, had
40 adverse effects on people's safety, lives and property (Yan et al., 2021). Scholars in
41 China have divided rainstorms caused by Meiyu fronts into three types (Zhang et al.,
42 2014). The first type is the β mesoscale convective rainstorm on the Meiyu front. This
43 type of rainstorm has a range of less than 300 km with strong intensity and a fast
44 formation process (He et al., 2007). It is difficult to forecast before 12 hours and can be
45 detected only by using radar to make a proximity forecast (Zhang et al., 2002). The
46 second type is the persistent rainstorm located in front of the high-altitude low-pressure
47 tank in the western part of the Meiyu front. It is characterized by a long duration of
48 approximately 5 days but appears less frequently, mainly in western Hubei and western
49 Hunan and Sichuan (Cai et al., 2021; Wu et al., 2020;). The last type is the rainstorm
50 caused by the Jianghuai cyclone located east of the origin of the Meiyu. The Jianghuai
51 cyclones are affected by the thermal conditions of the sea and land and likely occur in
52 the eastern part of the Meiyu front (Wang et al., 2016). The positive vorticity advection
53 in front of the high-altitude trough and the warm advection in front of the front promote
54 the eastward movement and development of the cyclone (Shen et al., 2019; Zhang et



55 al., 2016). During the development of the cyclone, the lower levels are dominated by
56 the southwest warm and humid airflow, and the high levels are mainly affected by dry
57 and cold air (Zhao et al., 2008). This type of rainstorm has a large range, high intensity
58 and long duration of precipitation (Wang et al., 2012; Xu et al., 2011).

59 Scholars' studies on Jianghuai cyclones during the Meiyu period were initially
60 based on individual case analysis. Xu et al. (2013) studied a cyclone process in 2011
61 and found that the cyclone process lasted up to 36 h. The cyclone rainstorm was
62 distributed on the south side of the cyclone. Heavy precipitation during the whole
63 cyclone mainly occurred in the lower reaches of the Yangtze River. Wu et al. (2020)
64 studied 2 different cyclone rainstorm processes. They found that rainfall is directly
65 proportional to cyclone intensity. There is a strong convergence center of water vapor
66 flux during cyclone development. Zhou et al. (2020) found that a tornado was generated
67 from the cyclone occlusion stage on July 22. The tornado was under the influence of a
68 strong and fast Jianghuai cyclone and produced heavy precipitation accompanied by
69 thunderstorm phenomena. With the improvement of cyclone identification methods and
70 reconstruction of reanalysis data, statistical studies of cyclones have been further
71 developed (Simmonds et al., 2000; Wernli et al., 2006). Yang et al. (2010) modeled the
72 rainstorm process in the lower reaches of the Yangtze River from 1998 to 2005. The
73 cyclones accounted for 62.5% of the rainstorm cases, and more than 70% of the
74 cyclones could develop and produce rainstorms. The Jianghuai cyclone located in the
75 lower reaches of the Yangtze River generally exists in the lower troposphere at 700 hPa.
76 The horizontal scale is within 400 km, and the life period on land is generally less than
77 48 h. Wang et al. (2015) found that the number of cyclones was lower and their intensity
78 was weak in the 1980s and 1990s. In the early 2000s, cyclones were more frequent, and
79 their intensity increased. After 2010, there was again a decreasing trend. Zhang et al.
80 (2018) divided 60 cases of extreme precipitation in the middle reaches of the Yangtze
81 River from 2008 to 2015 into five types. Among them, the extreme precipitation of the
82 Jianghuai cyclone type accounted for 30%. The stable and maintained Western Pacific
83 subtropical high (WPSH) system is one of the important reasons for the strong



84 precipitation produced by cyclones. Because of the weak cold air force, the intensity of
85 the Jianghuai cyclone is weaker than that in spring (Zhou et al., 2017). The daily
86 analysis of the Jianghuai cyclones in the Meiyu period is easy to ignore. All these
87 studies indicate that the Jianghuai cyclone is an important weather system that causes
88 heavy rainfall during the Meiyu period in the middle and lower reaches of the Yangtze
89 River (Wu et al., 2021; Zhang et al., 2018; Zhu et al., 1998).

90 Research on the climatic characteristics and precipitation effects of Jianghuai
91 cyclones during the Meiyu period in the past 60 years has not yielded clear results. In
92 this study, the relative vorticity method is used to objectively identify and track
93 cyclones based on reanalysis data provided by ERA5. The climatological characteristics
94 of the Jianghuai cyclones during this period are studied. We analyze the correlation
95 between Jianghuai cyclone activity and precipitation. This study provides a reference
96 for the long-term and short-term forecasting of precipitation in the Meiyu period.

97 The remainder of the present paper is organized as follows. Section 2 of this paper
98 presents the dataset and analytical methods. In Section 3, we show the climatology
99 composite of the cyclone tracks, genesis locations, intensity, lifetime and so on. There
100 is a positive correlation between the frequency of cyclonic activity and precipitation in
101 the Meiyu period. The relationship between them is studied by means of the
102 geopotential height anomaly and water vapor flux anomaly. Section 4 provides the main
103 discussion and findings of this study.

104 **2. Data and methods**

105 **2.1 Data**

106 The time span of all the data is 60 years from 1961 to 2020, and the study area is
107 located at 108°E-123°E, 27°N-34°N. We use the ERA5 relative vorticity hourly data
108 (850 hPa) released by the European Centre for Medium Range Weather Forecasts
109 (ECMWF) for Jianghuai cyclone identification and tracking. The spatial resolution of
110 the data is 0.25°×0.25°, and the temporal resolution is 6 h. Every 6 h was defined as a
111 step. The data of geopotential height, wind field, and specific humidity are daily data



112 processed from ERA5 hourly data with a spatial resolution of $0.25^{\circ} \times 0.25^{\circ}$ (Hersbach
113 et al., 2018). The geopotential height and wind field data include pressure levels of
114 approximately 500 hPa, 700 hPa and 850 hPa. The specific humidity data include
115 pressure levels of approximately 500 hPa, 700 hPa and 850 hPa. The precipitation data
116 are from the CN05.1 grid point observation dataset compiled by the National
117 Meteorological Information Center with a resolution of $0.25^{\circ} \times 0.25^{\circ}$.

118 **2.2 Methods**

119 The objective identification and tracking method for cyclones used in this paper is
120 the vorticity tracking method proposed by Hodges (1994, 1995). The first step is to use
121 the relative vorticity field at the 850 hPa pressure level corresponding to every moment
122 of the cyclone to determine the range of each cyclone. The second step is to find the
123 feature points. In the process of finding the feature points, the extreme point and the
124 centroid point are the alternatives. Corresponding to the global relative vorticity grid
125 data of each time point, several feature points can be found, and each point represents
126 a cyclone. The third step is to match the track of each cyclone under the given time
127 span. In Hodges (1994), the assumed data used are defined on a rectangular grid, and
128 each time step is initially processed to identify the maximum or minimum value of the
129 "object" on the positioning grid. The tracking method is feasible on high-resolution
130 grids, but on low-resolution grids, the feature points may not be sufficient to produce
131 smooth trajectories, so the smoothness of the tracking algorithm is effectively limited.
132 Hodges (1995) proposed tracking feature points on the unit sphere, which would
133 become the feature point matching problem of grid data for adjacent time points in
134 cyclone tracking. If the algorithm is reasonable, there is no "discontinuity" mutation in
135 the final arriving cyclone track, and the track is more accurate.

136 In addition to the relative vorticity method of tracking proposed by Hodges,
137 different methods of cyclone identification have also been proposed by other scholars.
138 Lu (2017) improved the extratropical cyclone identification and tracking method
139 involving the nine-point pressure minimum. Jiang et al. (2020) proposed an algorithm



140 for identifying extratropical cyclones on the basis of gridded data. This algorithm is
141 named the eight-section slope detection method.

142 Based on many different methods of objective cyclone identification, we chose the
143 relative vorticity tracking method. The relative vorticity tracking method can detect low
144 vortex systems earlier and track cyclones for a longer period of time with better stability.
145 When the closed pressure levels are not visible on the satellite map, the vorticity
146 tracking method can still continue to track the cyclone, improving the accuracy of
147 cyclone track data.

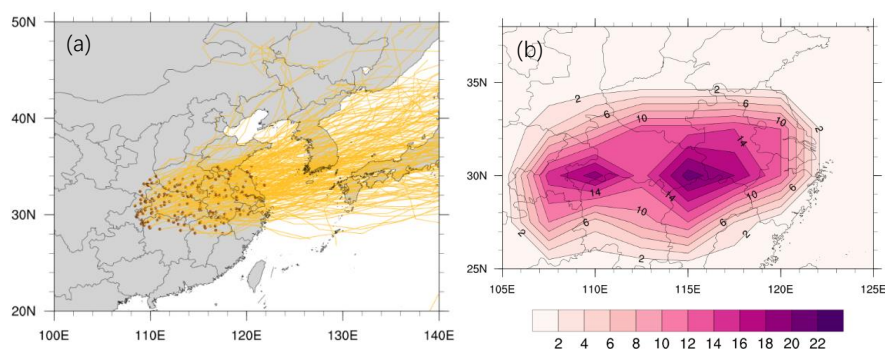
148 **3. Results**

149 **3.1 Climatic characteristics of the Jianghuai cyclone during the Meiyu period**

150 A total of 202 Jianghuai cyclones existed during the Meiyu period from 1961 to
151 2020. The range of cyclone genesis locations defined by the Jiangsu Meteorological
152 Administration (2017) and the characteristics of the relative vorticity tracking method
153 were used. We adjust the genesis location and remove the cyclones that are generated
154 at sea and have no effect on land precipitation (108°E-123°E, 27°N-34°N). Figure 1a
155 shows the distribution of Jianghuai cyclone tracks. The brown dots represent the genesis
156 locations of the first occurrence of the Jianghuai cyclone. The yellow lines indicate the
157 tracks of the cyclones. As shown in the figure, the tracks of the cyclone are mainly
158 eastward and northeast. These two kinds of tracks are related to the upper-level guide
159 airflow of 500~700 hPa (Wei et al., 2013). The northeast track is mainly due to the
160 southwest warm and moist air on the edge of the WPSH. The east track is mainly related
161 to the location of the WPSH. Figure 1b shows the frequency of cyclone genesis
162 locations during the Meiyu period from 1961 to 2020. The genesis locations of cyclones
163 are mainly located in the middle and lower reaches of the Yangtze River and the Huaihe
164 River basin, with an east–west band distribution (Wang et al., 2015; Wu et al., 2020).
165 The frequency of occurrence is higher in the region of the Hubei and Chongqing
166 junction, eastern Hubei, northern Jiangxi, south-central Anhui, Jiangsu and Zhejiang.
167 Research has found that the genesis locations of cyclones are closely related to the



168 landform (Xu 2021; Zhang et al., 2012).



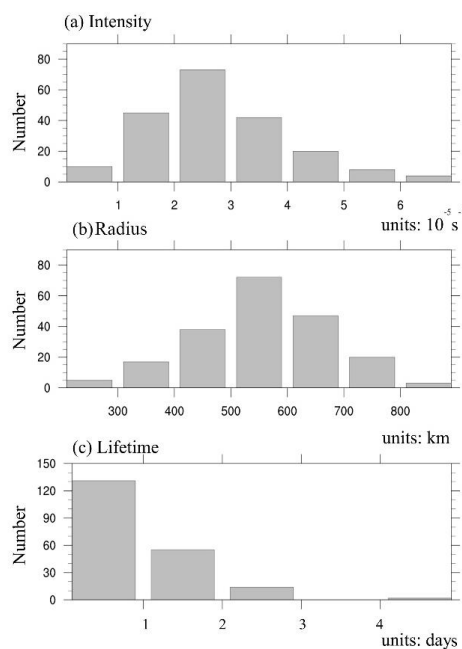
169 Fig 1. Distribution of the cyclone genesis locations and the cyclone tracks during the
170 1961-2020 Meiyu period (a). (The brown dots represent the genesis locations. The
171 yellow lines indicate the tracks). The frequency of genesis locations for the selected
172 cyclones during the Meiyu period from 1961 to 2020 (b).

173 To examine the climatological characteristics of Jianghuai cyclones over 60 years,
174 we focus on the intensity, radius, and lifetime of cyclones on land. The intensity of the
175 Jianghuai cyclone is defined as the relative vorticity intensity of the 850 hPa cyclone
176 center. The larger the relative vorticity intensity is, the stronger the cyclone intensity is.
177 Figure 2a shows that among the 202 selected cyclones, the intensity of the cyclone
178 center mainly ranges from $0 \times 10^{-5} \text{ s}^{-1}$ to $7 \times 10^{-5} \text{ s}^{-1}$. When the intensity of the cyclone
179 center is less than $3 \times 10^{-5} \text{ s}^{-1}$, the number of cyclones increases with increasing intensity;
180 when it is larger than $3 \times 10^{-5} \text{ s}^{-1}$, the number of cyclones decreases with weakening
181 intensity. The number of cyclones in the range of $2 \times 10^{-5} \text{ s}^{-1}$ to $3 \times 10^{-5} \text{ s}^{-1}$ has the largest
182 proportion, accounting for 36% of the total number of cyclones. A total of 180 cyclones
183 are in the range of $1 \times 10^{-5} \text{ s}^{-1}$ to $5 \times 10^{-5} \text{ s}^{-1}$ in intensity, accounting for 89%. Figure 2b
184 shows the relationship between the radius of cyclones and the number of cyclones. Most
185 of the cyclones have an average radius between 300 and 800 km, accounting for 96%
186 of the total number. The number of cyclones with radii between 500 and 600 km is the
187 largest, accounting for 35%. Figure 2c shows the relationship between the time of
188 cyclones affecting precipitation on land and the number of cyclones. Most of the

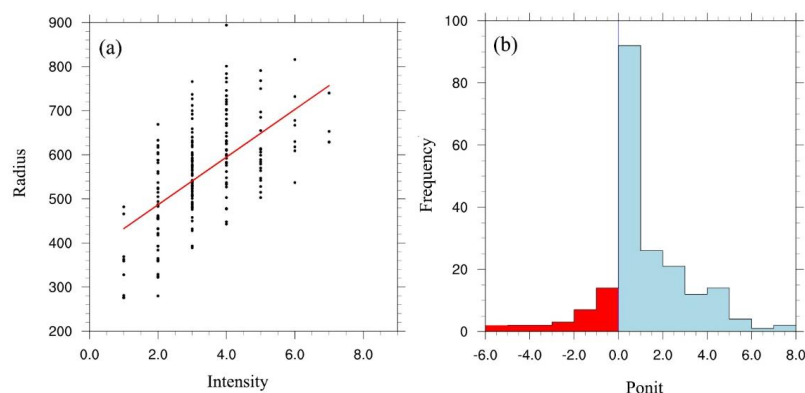


189 cyclones affect precipitation on land for 1-3 days, and only one cyclone affects
190 precipitation on land for more than 3 days. The number of cyclones that affected
191 precipitation on land within 2 days was 186, accounting for 92% of the total number.

192 The intensity of a cyclone is one of the factors affecting its precipitation and impact
193 range during the Meiyu period (Zhao et al., 2010). Figure 3a shows a positive
194 correlation between the maximum intensity and the maximum radius of cyclone
195 development. The stronger the intensity of a cyclone is, the larger its radius. Therefore,
196 the horizontal scale of most strong cyclones is larger than that of weak cyclones, the
197 precipitation is greater, and the precipitation range is larger. From the distribution of the
198 time lag between the maximum intensity and the radius of the cyclone shown in Figure
199 3b, the number of cyclones that reach both at the same time accounts for 45% of the
200 total number of cyclones. Of the remaining Jianghuai cyclones, more reach the
201 maximum intensity first and then continue to develop to the maximum horizontal scale.

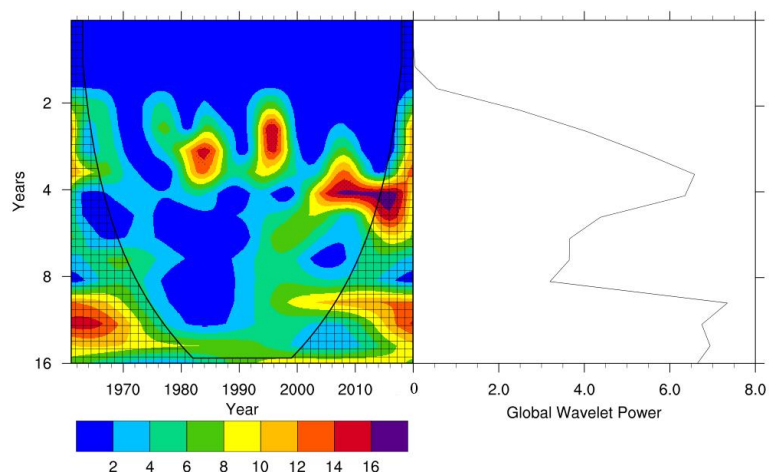


202 Fig 2. Distributions of the number of selected cyclones versus their (a) intensities (units:
203 10⁻⁵ s⁻¹), (b) radii (units: km), and (c) lifetimes (units: days).



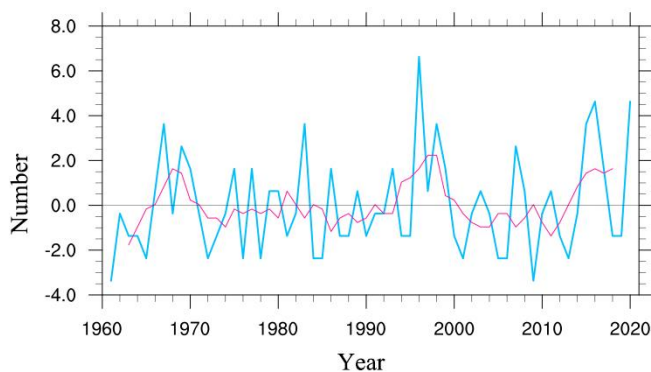
204 Fig 3. Correlation between maximum intensity (units: 10^{-5} s^{-1}) and maximum radius
205 (units: km) (a) and their time lag during the development of the Jianghuai cyclone in
206 the Meiyu period (b).

207 The frequency of Jianghuai cyclone occurrence is characterized by multiperiod
208 variation (Figure 4). The shaded area in the figure indicates that the 95% confidence
209 interval is passed. Strong 2–4-year quasiperiodic variation is observed for 1980-1990
210 and 1990-2000. After 2000, the quasiperiodic change in cyclones is approximately 4-5
211 years. This change period corresponds to the period of abnormal change in Meiyu. Chen
212 et al. (2019) pointed out that 3~4 years of quasiperiodic change is the main component
213 of abnormal changes in Meiyu when studying the quasiperiodic change in Meiyu. This
214 quasiperiodic variation component is mainly influenced by the out-of-ocean forcing of
215 the Indian Ocean dipole (IOP), which changes from the ENSO in the previous winter
216 to late spring and early summer with seasonal changes (Liang et al., 2018). During the
217 positive phase of the IOP, the strong warming of the Indian Ocean triggers a strong
218 Indian monsoon. This leads to a strengthening of the WPSH and an increase in
219 precipitation in southern China. The southwestern rapids, which are enhanced by the
220 positive IOP, also provide sufficient water vapor and warm advection to generate
221 favorable conditions for the development of the Jianghuai cyclone.



222 Fig 4. Periodic wavelet analysis diagram of Jianghuai cyclones during the Meiyu period
223 from 1961 to 2020 (shadow indicates passing the 95% confidence interval).

224 Jianghuai cyclones are not only characterized by multiperiod variability but also
225 have significant interdecadal variability. Figure 5 shows the activity frequency anomaly
226 and 5-year sliding average of cyclones during the Meiyu period from 1961 to 2020. The
227 frequency of cyclone activity was the highest in 1996 and the lowest in 1961 and 2009.
228 In the long term, the frequency of cyclone activity in the middle and lower reaches of
229 the Yangtze River increased in 1965-1970, in 1990-2000 and after 2010. It decreased
230 in 1970-1990 and 2000-2010. The interdecadal variability trend of Jianghuai cyclones
231 is similar to the interdecadal variability trend of precipitation during the Meiyu period
232 (Chen et al., 2019).

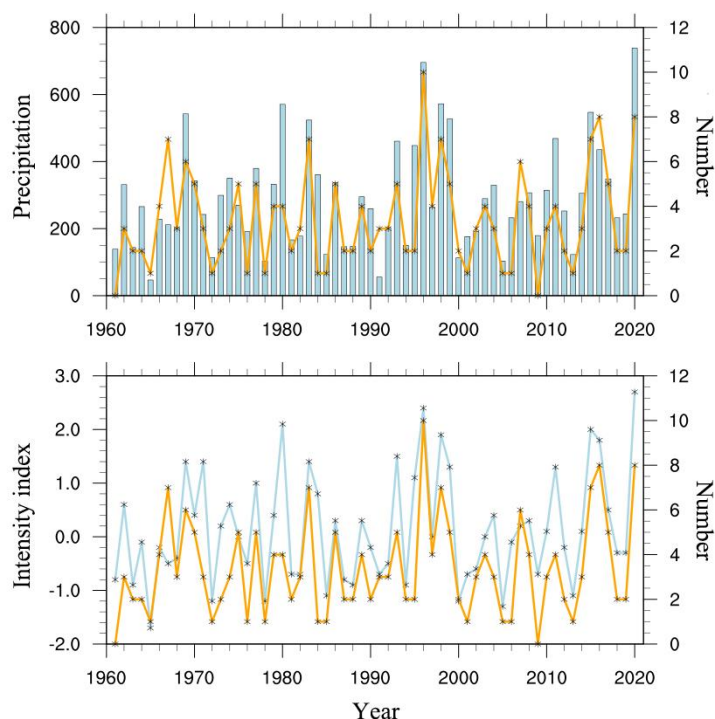




233 Fig 5. Frequency anomaly and 5-year sliding average of cyclones. The blue line
234 shows the anomalies in the number of cyclones, and the pink line shows the 5-year
235 sliding average of the anomalies.

236 **3.2 Linkage between cyclone activity and concurrent rainfall in the middle and** 237 **lower reaches of the Yangtze River.**

238 The Jianghuai cyclones are mainly active in the middle and lower reaches of the
239 Yangtze River (Huang et al., 2019; Li et al., 2002). Under the influence of the
240 strengthening westward extension of the WPSH during the Meiyu period, the Jianghuai
241 cyclones are restricted from entering the sea to some extent (Qin et al., 2015; Wu et al.,
242 2020). They form rainstorms and gales in the middle and lower reaches of the Yangtze
243 River and the coastal areas. A large part of the precipitation in the Meiyu period comes
244 from cyclone precipitation (Zhang et al., 2018). The intensity of Meiyu is usually
245 expressed by the Meiyu intensity index. The intensity of precipitation is affected not
246 only by precipitation but also by the number of precipitation days in the Meiyu period.
247 Both jointly determine the intensity of Meiyu in that year. The time-series plots of the
248 number of cyclones related to precipitation and the intensity index during the Meiyu
249 period from 1961 to 2020 are given in Figure 6a and 6b. We found that the number of
250 cyclones has a positive correlation coefficient of 0.769 with precipitation in the Meiyu
251 period (passing the 99% confidence interval). The number of cyclones was also
252 positively correlated with the Meiyu intensity index, with a correlation index of 0.760
253 (passing the 99% confidence interval). The frequency of Jianghuai cyclone activity in
254 years with a strong Meiyu index is high; the frequency of Jianghuai cyclone activity in
255 years with a weak Meiyu index is low.



256 Fig 6. (a) Changes in precipitation (blue bar chart) (unit: mm/day) and the number of
257 cyclones (orange line); (b) intensity index (blue line) and the number of cyclones
258 (orange line) in the Meiyu period from 1961 to 2020.

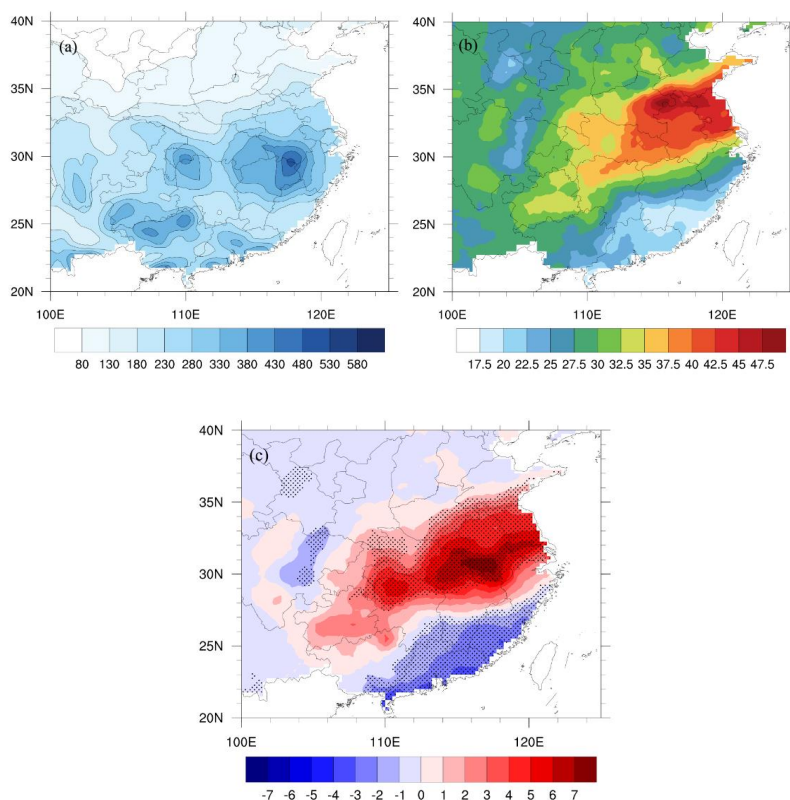
259 Figure 7a shows the spatial distribution of annual average precipitation during the
260 Meiyu period from 1961 to 2020. The areas with large precipitation values in the middle
261 and lower reaches of the Yangtze River are mainly located in the Dabie Mountains of
262 Anhui Province, the northern part of Jiangxi Province, the eastern part of Hubei
263 Province and the western part of Hubei Province. The maximum annual average
264 precipitation during the Meiyu period in southern Anhui can even exceed 480 mm. The
265 occurrence of large precipitation areas during the Meiyu period is closely related to the
266 topography of the region (Wu et al., 2023).

267 If precipitation and Jianghuai cyclone activity existed on the same day during the
268 Meiyu period, we defined that day as a Jianghuai cyclone precipitation day. The
269 remaining days in the Meiyu period were treated as non-Jianghuai cyclone precipitation



270 days. Figure 7b shows the spatial distribution of the proportion of cyclone precipitation
271 relative to total precipitation during the Meiyu period. As shown in the figure, the main
272 areas affected by cyclone precipitation are the middle and lower reaches of the Yangtze
273 River. The Huaihe River basin in northern Anhui Province is the most affected area.
274 The cyclone precipitation in the Huaihe River basin accounts for more than 47% of the
275 total precipitation during the Meiyu period, while the cyclone-influenced precipitation
276 in other areas accounts for more than 35% of the total precipitation. In general, the
277 degree of cyclone-influenced precipitation in the middle and lower reaches of the
278 Yangtze River shows an east–west band distribution and a gradual decrease from
279 coastal to inland areas. This indicates that the distribution of the large-value area and
280 the characteristics of the band distribution are related to the northeast and eastward
281 tracks of the Jianghuai cyclone. Its precipitation capacity gradually increases with the
282 development of cyclone movement.

283 Figure 7c shows the spatial distribution of the daily mean precipitation anomaly
284 of the Jianghuai cyclone (the shaded part indicates that the 95% confidence interval is
285 passed). When the Jianghuai cyclone is active, the middle and lower reaches of the
286 Yangtze River to the east of 108°E show an abnormal increase in precipitation. However,
287 Fujian, Guangdong and other places show an abnormal decrease. Among them, the
288 maximum value of abnormally increased precipitation can exceed 7 mm/day in areas
289 such as southern Anhui, eastern Hubei and northern Jiangxi. The large-value areas of
290 precipitation anomalies are consistent with the large-value areas of cyclone occurrence
291 frequency sources. It is inferred that the spatial distribution of precipitation anomalies
292 has a connection with the distribution of cyclone genesis locations. This phenomenon
293 of increasing and decreasing precipitation anomalies is bounded by approximately
294 27°N and distributed north–south in the form of dipoles.



295 Fig 7. (a) Annual mean precipitation during the Meiyu period from 1961 to 2020 (unit:
296 mm/year); (b) proportion of Jianghuai cyclone precipitation relative to total
297 precipitation during the Meiyu period (unit: %); (c) daily mean precipitation anomaly
298 of the Jianghuai cyclone during the Meiyu period (unit: mm/day) (shadow indicates
299 passing the 95% confidence interval).

300 Figure 8 shows the evolution of composite geopotential height and horizontal wind
301 anomalies for three different levels of Jianghuai cyclones from day -4 to +2 during the
302 Meiyu period. Day 0 is the day on which the cyclone first appears in the specified area.
303 Most areas of the lower and middle troposphere (700 hPa, 850 hPa) in the middle and
304 lower Yangtze River on day 0 are covered by significant negative geopotential height
305 anomalies with peak magnitudes greater than -11 gpm. There is a significant positive
306 geopotential height anomaly with a peak magnitude of over 13 gpm on the southeast



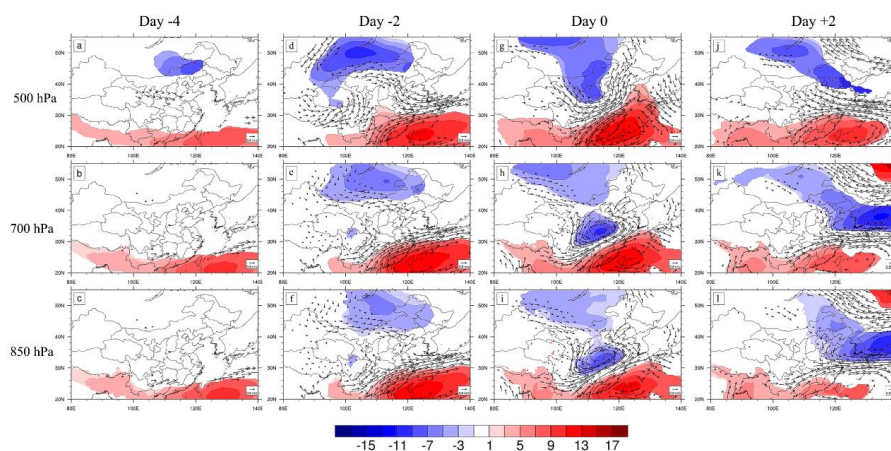
307 side of the negative geopotential height anomaly. These anomalies form meridional
308 dipole structures in the middle and lower troposphere geopotential height field. The
309 southwest wind anomaly is significant in the middle and lower reaches of the Yangtze
310 River. The south of Anhui Province and the north of Jiangxi Province are between the
311 positive geopotential height anomaly and negative geopotential height anomaly. The
312 existence of these anomalies indicates the enhancement of southwest winds and the
313 strengthening of the WPSH. The negative geopotential height anomalies at 500 hPa
314 height on day 0 are mainly in Mongolia, Shanxi and other places. Strong southwest
315 wind anomalies exist between the positive and negative geopotential height anomalies.
316 The negative geopotential height anomalies in the Mongolian region exceed -7 gpm.

317 The negative geopotential height anomalies on all three isobaric surfaces can be
318 traced back to Mongolia, Inner Mongolia and part of Northeast China on day -2.
319 Negative geopotential height anomalies at 500 hPa can be traced to day -4. On day -4,
320 significant southwestern wind anomalies exist in southwestern Hunan at 700 hPa and
321 850 hPa. Significant northwest wind anomalies exist in the Yellow River basin of China
322 at 500 hPa. By day -2, the negative geopotential height anomalies in Mongolia, Inner
323 Mongolia and some northeastern areas are enhanced for all three isobars. The positive
324 geopotential height anomalies of the WPSH are enhanced and extend northward to the
325 southern part of the middle and lower reaches of the Yangtze River. There are
326 significant southwest wind anomalies at the three isobaric surfaces in the south of the
327 middle and lower reaches of the Yangtze River, while there are significant northwest
328 wind anomalies at 500 hPa in the north of Anhui Province and Jiangsu Province. The
329 negative geopotential height anomalies on the three isobaric surfaces move eastward
330 with the formation and development of Jianghuai cyclones. On day +2, the lower
331 reaches of the Yangtze River are mainly affected by the combined action of anomalous
332 southwest winds and northwest winds. The positive geopotential height anomaly of the
333 WPSH is weakened.

334 Therefore, the abnormal precipitation caused by the Jianghuai cyclone mainly
335 comes from the abnormal southwest winds and the strengthening of the WPSH



336 (Rodwell et al., 1996; Sardeshmukh et al., 1998). The enhanced negative geopotential
 337 anomaly over Mongolia provides cold and dry air brought by the westerly jet for
 338 cyclone development. The enhanced southwest jet provides sufficient warm and moist
 339 air for the formation of cyclones and promotes the eastward migration of cyclones after
 340 formation. The increasing frequency of cyclones over the Yangtze River and Huaihe
 341 River leads to the abnormal increase in precipitation in the middle and lower reaches of
 342 the Yangtze River during the Meiyu period. However, due to the strengthening of the
 343 WPSH, the southern part of China is controlled by the abnormal positive geopotential
 344 height, and the precipitation decreases (Liu et al., 2020).



345 Fig 8. Evolution of composite geopotential height anomalies (shading; units: gpm) and
 346 horizontal wind anomalies (units: m/s) on the 850 hPa, 700 hPa, and 500 hPa isobaric
 347 surfaces for day -4 (a-c), day -2 (d-f), day 0 (g-i) and day +2 (j-l) for the 202 selected
 348 Jianghuai cyclones. Shading indicates that composite geopotential height anomalies are
 349 significant at the 95% confidence level based on a T test. Vectors are plotted if wind
 350 anomalies are significant at the 95% confidence level based on a T test in at least one
 351 direction.

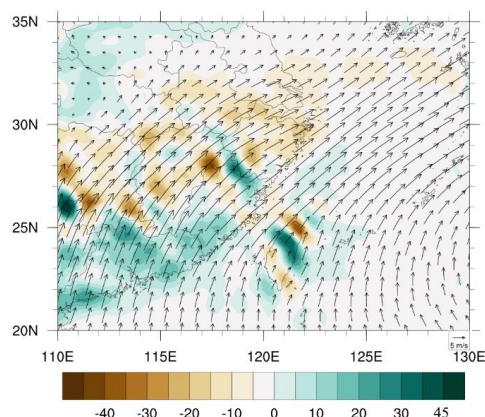
352 Figure 9 shows the climatic distribution of water vapor flux and water vapor flux
 353 divergence at a pressure level of 850 hPa during the Meiyu period. The water vapor
 354 involved in the precipitation process of the Jianghuai cyclone during the Meiyu period



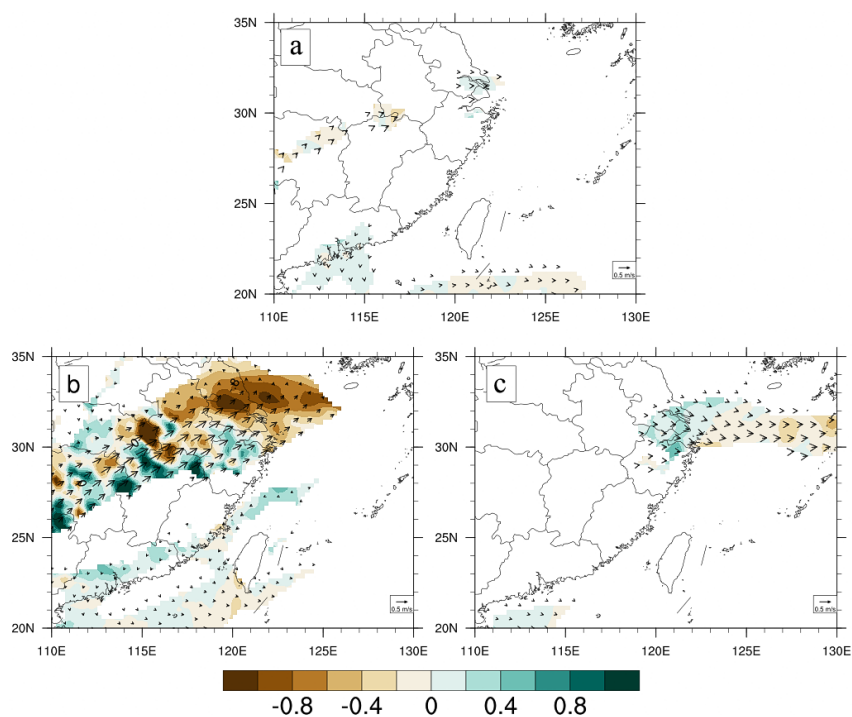
355 mainly comes from the water vapor brought by the southwest jet of the summer
356 monsoon in the low-latitude area. During Jianghuai cyclone development, the middle
357 and lower reaches of the Yangtze River are mostly in the water vapor convergence area,
358 which is conducive to the generation of precipitation (Chen et al., 2020).

359 Figure 10 shows the distribution of water vapor flux anomalies and water vapor
360 flux divergence anomalies at the pressure level of 850 hPa during the Jianghuai cyclone
361 from day -2 to day +2. The color field and wind vector arrows in the figure both passed
362 the 95% significance test. On day -2, a significant water vapor convergence anomaly
363 and water vapor transport in the southwest direction appear in southern Anhui Province.
364 The anomalies of water vapor flux and water vapor flux dispersion are mainly
365 concentrated on day 0. There is significant anomalous water vapor convergence up to -
366 $1 \text{ g} \cdot \text{cm}^{-2} \cdot \text{hPa}^{-1}$ in eastern Hubei Province, Anhui Province and Jiangsu Province on day
367 0. Anomalous water vapor dispersion exists in the southern part of the middle and lower
368 reaches of the Yangtze River and some areas in southern China. On day +2, with the
369 development of the cyclone's eastward movement, only the southern part of Jiangsu
370 Province and the northern part of Zhejiang Province have abnormal water vapor flux in
371 the eastward direction. The precipitation in the area begins to gradually weaken at this
372 time.

373 From day -2 to day 0, the abnormal water vapor flux and water vapor flux
374 divergence configuration make the warm and wet air in the low-latitude area transport
375 to the middle and lower reaches of the Yangtze River. The abnormal water vapor flux
376 has a negative value, water vapor convergence occurs, local water vapor volume
377 increases, and finally, the precipitation in the region increases. In contrast, the anomaly
378 of water vapor flux in southern Guangdong and other regions is divergent. This leads
379 to a decrease in local water vapor volume and precipitation in this region. These results
380 indicate that the variations in water vapor flux and divergence related to cyclones are
381 mainly from warm and wet air transported from low latitudes to the middle and lower
382 reaches of the Yangtze River. Therefore, there is a positive correlation between cyclone
383 activity and precipitation in the middle and lower reaches of the Yangtze River.



384 Fig 9. Distribution of 850 hPa daily mean water vapor flux (unit: $\text{g}\cdot\text{cm}^{-2}\cdot\text{hPa}^{-1}$) and
385 water vapor flux divergence (unit: $10^{-8} \text{g}\cdot\text{cm}^{-2}\cdot\text{hPa}^{-1}\cdot\text{s}^{-1}$) of cyclones over the Yangtze
386 and Huaihe rivers during 1961-2020 (color diagram shows water vapor flux divergence,
387 and vector diagram shows water vapor flux). The colored region passed the 95%
388 confidence interval according to a T test. If the vapor flux anomaly is significant at the
389 95% confidence level for the T test in at least one direction, the vector is plotted.





390 Fig 10. Distribution of the 850 hPa daily mean water vapor flux anomaly (unit: $\text{g}\cdot\text{cm}^{-2}\cdot\text{hPa}^{-1}$) and water vapor flux divergence anomaly (unit: $10^{-8}\text{ g}\cdot\text{cm}^{-2}\cdot\text{hPa}^{-1}\cdot\text{s}^{-1}$) of
391 cyclones over the Yangtze and Huaihe rivers during 1961-2020 (color diagram shows
392 water vapor flux divergence, and vector diagram shows water vapor flux). The colored
393 region passed the 95% confidence interval according to a T test. If the vapor flux
394 anomaly is significant at the 95% confidence level for the T test in at least one direction
395 (zonal or meridian), the vector is plotted.
396

397 **4. Summary and discussion**

398 Based on ERA5 reanalysis of sea level pressure data and using the relative
399 vorticity method to identify and track cyclones, we have examined the impacts of the
400 climatological characteristics of Jianghuai cyclones. The linkages between cyclone
401 activity and precipitation in the middle and lower reaches of the Yangtze River during
402 the Meiyu period are also analyzed.

403 During the Meiyu period, Jianghuai cyclones are mainly generated at the junction
404 of western Hubei and Chongqing Municipality, eastern Hubei Province, northern
405 Jiangxi Province, central and southern Anhui Province, and Jiangsu and Zhejiang
406 provinces. These cyclones develop and move to the sea in the east or northeast direction.
407 There is a positive correlation between the maximum intensity and maximum radius of
408 Jianghuai cyclones. The higher the cyclone intensity is, the larger the radius will be. Its
409 occurrence frequency not only has the characteristics of multicycle variation but also
410 has obvious interdecadal variation, which has a good correspondence with the periodic
411 and interdecadal variation in precipitation in the Meiyu period.

412 There is a positive correlation between the frequency of cyclone activity and
413 precipitation in the Meiyu period. The frequency of Jianghuai cyclone activity is high
414 in the years with strong Meiyu rainfall and low in the years with weak Meiyu rainfall.
415 The percentage of precipitation affected by Jianghuai cyclone activity in the middle and
416 lower reaches of the Yangtze River can reach up to 47%. The spatial distribution is in
417 the shape of an east–west belt, and the degree of influence gradually decreases from the



418 coast to the interior. When the Jianghuai cyclone is active, the precipitation increases
419 abnormally in the middle and lower reaches of the Yangtze River east of 108°E.
420 Precipitation decreases abnormally in Fujian Province and Guangdong Province. The
421 spatial distribution of precipitation anomalies is related to the genesis locations of
422 cyclone frequency, and the positive and negative anomalies are distributed north–south
423 in the form of dipoles based on the latitude line at approximately 27°N as the boundary.

424 The geopotential height anomaly field and the horizontal wind vector anomaly
425 field of the Jianghuai cyclones during the Meiyu period are synthesized and analyzed.
426 There is an enhanced positive geopotential height anomaly of the WPSH during cyclone
427 activity. The negative geopotential altitude anomaly of Mongolia and the abnormal
428 southwest jet are enhanced. All of these factors lead to an increase in precipitation in
429 the middle and lower reaches of the Yangtze River. The abnormal leading signal of the
430 negative geopotential height in Mongolia can be traced to day -2 of the cyclone activity,
431 and the signal can be traced to day -4 at 500 hPa. From day -2 to day 0 of cyclone
432 activity, the abnormal distribution of water vapor flux and water vapor flux divergence
433 cause the warm and wet air at the low latitudes to be transported to the middle and lower
434 reaches of the Yangtze River. They promote the generation and development of
435 cyclones and increase precipitation in the middle and lower reaches of the Yangtze
436 River. It is worth noting that different intensities of Jianghuai cyclones in the middle
437 and lower reaches of the Yangtze River may have different impacts on precipitation.
438 The specific mechanism by which the southwest jet affects cyclones during the Meiyu
439 period is not clear enough. These problems need further analysis and research.

440 **Competing interests**

441 The contact author has declared that none of the authors has any competing interests.



442 **References**

- 443 Bao, Y, Y.: Similarities and Differences of Monsoon Circulations between 2016 and
444 1998 Meiyu Periods in Middle and Lower Reaches of the Yangtze River and
445 Comparison of Their Physical Mechanisms. Chinese Journal of Atmospheric
446 Sciences., 45, 994–1006, 2021. DOI: [10.3878/j.issn.1006-9895.2101.20174](https://doi.org/10.3878/j.issn.1006-9895.2101.20174)
- 447 Cai, Y, X., He, H., Lu, H., Zhu, L, Y., and Lu, Q, Q.: Synoptic and climatic
448 characteristics of persistent rainstorm in Guangxi in June 2020. Journal of
449 Meteorological Research and Application., 4, 113-117, 2021.
450 DOI:[10.19849/j.cnki.CN45-1356/P.2021.1.20](https://doi.org/10.19849/j.cnki.CN45-1356/P.2021.1.20).
- 451 Chen, L, J., Zhao, J, H., Gu, W., Liang, P., Zhi, R., Peng, J, B., Zhao, S, Y., Gao, H., Li,
452 X. and Zhang, P, Q.: Advances of Research and Application on Major Rainy Seasons
453 in China. Journal Of Applied Meteorological Science., 30, 385-400, 2019.
454 DOI: [10.11898/1001-7313.20190401](https://doi.org/10.11898/1001-7313.20190401)
- 455 Chen, T., Zhang, F, H., Yu, C., Ma, J., Zhang, X, D., Shen, X, L., Zhang, F. and Luo,
456 Q.: Synoptic analysis of extreme Meiyu precipitation over Yangtze River Basin during
457 June-July. Meteor Mon., 46, 1415-1426, 2020.
458 DOI: [10.7519/j.issn.1000-0526.2020.11.003](https://doi.org/10.7519/j.issn.1000-0526.2020.11.003)
- 459 Ding, Y, H.: Summer monsoon rainfalls in China. J Meteor Soc Jpn.,70, 373-396, 1992.
460 DOI: https://doi.org/10.2151/jmsj1965.70.1B_373
- 461 Ding, Y, H.: Seasonal march of the east-Asian summer monsoon. Chang C P. East Asian
462 Monsoon. Hackensack: World Scientific., 64, 2004.
463 DOI: https://doi.org/10.1142/9789812701411_0001
- 464 He, L, F., Chen, T., Zhou, Q, L. and Li, Z, C.: The Meso- β Scale Convective System of
465 a Heavy Rain Event on July 10, 2004 in Beijing. Journal Of Applied Meteorological
466 Science., 18, 655-665, 2007. DOI: [10.3969/j.issn.1001-7313.2007.05.010](https://doi.org/10.3969/j.issn.1001-7313.2007.05.010)
- 467 Hersbach, H., and Coauthors.: ERA5 hourly data on pressure levels from 1940 to
468 present. Copernicus Climate Change Service (C3S) Climate Data Store (CDS)., 2018.
469 DOI: [10.24381/cds.bd0915c6](https://doi.org/10.24381/cds.bd0915c6)
- 470 Hodges, K. I.: A general method for tracking analysis and its application to



- 471 meteorological data. Monthly Weather Review., 122, 2573-2586, 1994.
472 DOI:[https://doi.org/10.1175/1520-0493\(1994\)122<2573:AGMFTA>2.0.CO;2](https://doi.org/10.1175/1520-0493(1994)122<2573:AGMFTA>2.0.CO;2).
- 473 Hodges, K, I.: Feature tracking on the unit sphere. Monthly Weather Review., 123,
474 3458-3465, 1995.
475 DOI:[https://doi.org/10.1175/1520-0493\(1995\)123<3458:FTOTUS>2.0.CO;2](https://doi.org/10.1175/1520-0493(1995)123<3458:FTOTUS>2.0.CO;2).
- 476 Huang, W, Y., Sun, Y., Lu, C, H., Yao, L, N. and Dong, Q.: Statical analysis of Jianghuai
477 cyclone causing Jiangsu regional heavy rain in summer nearly 40 years. Meteor Mon.,
478 45, 843-853, 2019. DOI: [10.7519/j.issn.1000-0526.2019.06.010](https://doi.org/10.7519/j.issn.1000-0526.2019.06.010)
- 479 Jiangsu Provincial Weather Bureau: Jiangsu Province Weather Forecast Techniacal
480 Manual. Beijing: China Meteorological Press., 22-33, 2017.
- 481 Li, B., Yu, W, P., Lu, Y. and Lu, D, C.: The numerical simulating study of the mesoscale
482 characteristics on development of Jianghuai cyclones. Science meteorologic., 22, 72-
483 80, 2002. DOI: [10.3969/j.issn.1009-0827.2002.01.009](https://doi.org/10.3969/j.issn.1009-0827.2002.01.009).
- 484 Liang, P., Chen, L, J., Ding, Y, H., He, J, H. and Zhou, B.: Relationship between long-
485 term variability of Meiyu over the Yangtze River and ocean and Meiyu's
486 predictability study. Acta Meteorologica Sinica., 76, 379-393, 2018.
487 DOI:[10.11676/qxxb2018.009](https://doi.org/10.11676/qxxb2018.009).
- 488 Liu, Y, Y., Ding, Y, H.: Characteristics and possible causes for extreme Meiyu in 2020.
489 Meteor Mon.,46, 1393-1404, 2020. DOI: [10.7519/j.issn.1000-0526.2020.11.001](https://doi.org/10.7519/j.issn.1000-0526.2020.11.001)
- 490 Lu, C, H.: A Modified Algorithm for Identifying and Tracking Extratropical Cyclones.
491 Advances in atmospheric sciences., 34, 909-924, 2017. DOI: [10.1007/s00376-017-6231-2](https://doi.org/10.1007/s00376-017-6231-2)
- 492
- 493 Pang, Y., Wang, L, J. and Yu, B.: The relationship between 10-30d low frequency
494 oscillation and the rainfall over Changjiang-Huaihe River valley during Meiyu
495 period. Trans Atmos Sci., 36, 742-750, 2013.
496 DOI: [10.3969/j.issn.1674-7097.2013.06.011](https://doi.org/10.3969/j.issn.1674-7097.2013.06.011)
- 497 Qin, T., Wei, L, X.: The statistic and variance of cyclones entering coastal waters of
498 china in 1979-2012. Acta Oceanologica Sinica., 2015.
499 DOI: [10.3969/j.issn.0253-4193.2015.01.005](https://doi.org/10.3969/j.issn.0253-4193.2015.01.005)



- 500 Rodwell, M, J., Hoskins, B, J.: Monsoons and the dynamics of deserts. *Quart J Roy*
501 *Meteor Soc.*, 122, 385-1404, 1996. <https://doi.org/10.1002/qj.49712253408>
- 502 Sardeshmukh, P, D., Hoskins, B, J.: The generation of global rotational flow by steady
503 idealized tropical divergence. *J Atmos Sci.*, 45, 1228-1251, 1988.
504 DOI:[10.1175/1520-0469\(1988\)045<1228:TGOGRF>2.0.CO;2](https://doi.org/10.1175/1520-0469(1988)045<1228:TGOGRF>2.0.CO;2)
- 505 Shen, Y., Sun, Y., Cai, N, H., Su, X. and Shi, D, W.: Analysis on the generation and
506 evolution of a Jianghuai Cyclone responsible for extreme precipitation event. *Meteor*
507 *Mon.*,45, 166-179, 2019. DOI: [10.7519/j.issn.1000-0526.2019.02.003](https://doi.org/10.7519/j.issn.1000-0526.2019.02.003)
- 508 Simmonds, I., Keay, K.: Mean Southern Hemisphere extratropical cyclone behavior in
509 the 40-year NCEP-NCAR reanalysis. *J Climate.*, 13, 873-885, 2000.
510 DOI: [10.1175/1520-0442\(2000\)013<0873:MSHECB>2.0.CO;2](https://doi.org/10.1175/1520-0442(2000)013<0873:MSHECB>2.0.CO;2)
- 511 Simmonds, I., Murray, R, J.: Southern extratropical cyclone behavior in ECMWF
512 analyses during the FROST special observing periods. *Weather& Fore-casting.*, 14,
513 878-891, 1999.
514 DOI:[10.1175/1520-0434\(1999\)014<0878:SECBIE>2.0.CO;2](https://doi.org/10.1175/1520-0434(1999)014<0878:SECBIE>2.0.CO;2)
- 515 Su, X., Kang, Z, M., Zhuang, X, R. and Chen, S, J.: Uncertainty analysis of heavy rain
516 belt forecast during the 2020 Meiyu period. *Meteor Mon.*, 47, 1336-1346, 2021DOI:
517 [10.7519/j.issn.1000-0526.2021.11.003](https://doi.org/10.7519/j.issn.1000-0526.2021.11.003).
- 518 Tao, S, Y., Ding, Y, H. and Zhou, X, P.: Study on heavy rain and severe convective
519 weather. *Chinese Journal of Atmospheric Sciences.*1979.
- 520 Wang, J, H., Niu, D., Ren, S, Y., Miao, C, S. and Song, P.: Comparative Study On
521 Development Of Different Deep Jianghuai Rivers Cyclones Entering the Sea and the
522 Influence of Environmental Factors. *Journal Of Tropical Meteorology.*, 31, 744-756,
523 2016. DOI: [10.16032/j.issn.1004-4965.2015.06.003](https://doi.org/10.16032/j.issn.1004-4965.2015.06.003).
- 524 Wang, Y, L., Wang, L, J.: Characteristics of southern cyclone activity and its influence
525 on precipitation in Yangtze River Basin. *Yangtze River.*, 43, 34-36,68, 2012. DOI:
526 [10.3969/j.issn.1001-4179.2012.09.009](https://doi.org/10.3969/j.issn.1001-4179.2012.09.009).
- 527 Wang, Y, L., Guan, Z, Y., Jin, D, C. and Ke, D.: Climatic characteristics and interannual
528 variations of cyclones over Changjiang-Huaihe River basin during late spring and



- 529 early summer from 1980 to 2012. *Trans Atmos Sci.*, 38, 354-361, 2015.
- 530 DOI: [10.13878/j.cnki.dqkxxb.20130413010](https://doi.org/10.13878/j.cnki.dqkxxb.20130413010)
- 531 Wang, L, J., Huang, Q, L., Li, Y. and Han, S, R.: Relationship between spatial
532 inhomogeneous distribution of Meiyu rainfall over the Yangtze-Huaihe River Valley
533 and previous SST. *Trans Atmos Sci*, 37, 313-322, 2014. DOI: [10.3969/j.issn.1674-7097.2014.03.008](https://doi.org/10.3969/j.issn.1674-7097.2014.03.008)
- 534
- 535 Wei, J, S., Liu, J, Y., Sun, Y. and Xu, Y, C.: Climate characteristics of Jiang-Huai
536 cyclone. *J Meteor Sci*, 33, 196-201, 2013. DOI: [10.3969/2012jms.0112](https://doi.org/10.3969/2012jms.0112)
- 537 Wernli, H., Schwierz, C.: Surface cyclone in the ERA-40 dataset (1958-2001). Part I:
538 Novel identification method and global climatology. *J Atmos Sci.*, 63, 2486-2507,
539 2006.
- 540 Wu, J, F., Xu, X, F., Zhao, W, R., Qing, Q. and Zou, L.: Characteristics of Persistent
541 Heavy Rainfall and Water Vapor Transport in Western Sichuan Plateau.
542 *Meteorological science and technology.*, 48, 704-716, 2020.
543 DOI:[10.19517/j.1671-6345.20190301](https://doi.org/10.19517/j.1671-6345.20190301).
- 544 Wu, Q., Chen, S, J., Bai, Y., Xia, L. and Wang, C, J.: Diagnostic analysis and numerical
545 simulation of a heavy rainstorm associated with the Jianghuai cyclone. *Journal of the*
546 *Meteorological Sciences.*, 41, 86-98, 2021. DOI: [10.12306/2020jms.0029](https://doi.org/10.12306/2020jms.0029).
- 547 Wu, Q., Liu, T., Zhang, B., Zhang, Y. and Wang, Y.: A Comparative Analysis of the
548 Heavy Rainstorm Processes of Two Jianghuai Cyclones. *Anhui Agri, Sci, Bull.*, 26,
549 161-171, 2020. DOI: [10.3969/j.issn.1007-7731.2020.09.058](https://doi.org/10.3969/j.issn.1007-7731.2020.09.058)
- 550 Wu, Q., Feng, J, W., Wang, Y., Chen, Y. and Zhang, L, T.: Spatial and temporal
551 distribution of cyclones over the Jianghuai River during 1979-2018. *Meteorology of*
552 *Shanxi.*, 06, 15-22, 2021. DOI: [10.3969/j.issn.1006-4354.2020.06.003](https://doi.org/10.3969/j.issn.1006-4354.2020.06.003)
- 553 Wu, T., Xu, G, Y., Li, S, J. and Wei, F.: Characteristics and Causes of a Mixed-Type
554 Convective Weather During the Formation and Development of a Jianghuai Cyclone
555 in Spring. *Advances in Meteorological Science and Technology.*, 48, 704-716, 2023.
556 DOI:[10.19517/j.1671-6345.20190301](https://doi.org/10.19517/j.1671-6345.20190301).
- 557 Xu, J., Zhou, C, Y. and Gao, T, C.: Analysis about Development Mechanism of



- 558 Jianghuai Cyclone in Meiyu Front and Its Relationship with Rainstorm. *Bulletin Of*
559 *Science and Technology.*, 29, 24-29,86, 2013.
560 DOI: [10.3969/j.issn.1001-7119.2013.05.006](https://doi.org/10.3969/j.issn.1001-7119.2013.05.006).
- 561 Xu, J, M.: Satellite Imagery Characteristics for Extratropical Cyclones and Meiyu Font.
562 *Advances in Meteorological Science and Technology.*, 11, 14-26, 2021. DOI:
563 [10.3969/j.issn.2095-1973.2021.03.003](https://doi.org/10.3969/j.issn.2095-1973.2021.03.003)
- 564 Xu, Y, C., Wei, J, S. and Zhu, W, J.: A numerical simulation and marine sensitive
565 experiments of Jiang-Huai cyclone. *J Meteor Sic.*, 31, 726-731, 2011.
566 DOI: [10.3969/j.issn.1009-0827.2011.06.008](https://doi.org/10.3969/j.issn.1009-0827.2011.06.008)
- 567 Yan, J, R., Wang, W, J., Zhang, H. and Shi, D, W.: Analysis of two rainstorm and gale
568 processes of Jianghuai cyclone in Jiangsu Province in 2019. *Journal of*
569 *Meteorological Research and Application.*, 42, 83-88, 2021.
570 DOI: [10.19849/j.cnki.CN45-1356/P.2021.2.16](https://doi.org/10.19849/j.cnki.CN45-1356/P.2021.2.16)
- 571 Yang, Y, M., Gu, W, L., Zhao, R, L. and Liu, J.: The statical analysis of vortex during
572 Meiyu season in the lower reaches of the Yangtze. *Quarterly Journal of Applied*
573 *Meteorology.*, 21, 11-18, 2010. DOI: [10.3969/j.issn.1001-7313.2010.01.002](https://doi.org/10.3969/j.issn.1001-7313.2010.01.002)
- 574 Zhao, B, K., Wu, G, X. and Yao, X, P.: A diagnostic analysis of potential vorticity
575 associated with development of a strong cyclone during the Meiyu period of 2003.
576 *Chinese Journal of Atmospheric Sciences.*, 32, 1241-1255, 2008.
577 Doi: [10.3878/j.issn.1006-9895.2008.06.02](https://doi.org/10.3878/j.issn.1006-9895.2008.06.02).
- 578 Zhao, B, k., Wan, R, J. and Lu, X, Q.: A Contrastive Analysis on the Causes of Strong
579 and Weak Cyclones over Yangtze-Huaihe River Valleys during the Meiyu Period in
580 Summer of 2003. *Plateau Meteorology.*, 29, 309-320, 2010.
- 581 Zhao, J, H., Chen, L, J. and Wang, D, Q.: Characteristics and causes analysis of
582 abnormal Meiyu in China in 2016. *Chinese Journal of Atmospheric Sciences.*, 42,
583 1055-1066, 2018. DOI: [10.3878/j.issn.1006-9895.1708.17170](https://doi.org/10.3878/j.issn.1006-9895.1708.17170)
- 584 Zhao, J, H., Zhang, H., Zuo, J, Q., Xiong, K, G. and Chen, L, J.: What Drives the Super
585 Strong Precipitation over the Yangtze–Huaihe River Basin in the Meiyu Period of
586 2020. *Chinese Journal of Atmospheric Sciences.*, 45, 1433–1450, 2021.



- 587 Doi:[10.3878/j.issn.1006-9895.2104.2101](https://doi.org/10.3878/j.issn.1006-9895.2104.2101).
- 588 Zhang, X, L., Tao, S, Y. and Zhang, S, L.: Three Types of Heavy Rainstorms Associated
589 with the Meiyu Front. Chinese Journal of Atmospheric Sciences, 28., 187-205, 2004.
590 doi: [10.3878/j.issn.1006-9895.2004.02.03](https://doi.org/10.3878/j.issn.1006-9895.2004.02.03)
- 591 Zhang, X, L., Tao, S, Y. and Zhang, Q, Y.: An Analysis on Development of MESO- β
592 Convective System along Meiyu Front Associated with Flood in Wuhan in 20-21
593 July 1998, Journal of Applied Meteorological Science., 13, 385-397, 2002. DOI:
594 [10.3969/j.issn.1001-7313.2002.04.001](https://doi.org/10.3969/j.issn.1001-7313.2002.04.001).
- 595 Zhang, X, H., Luo, J., Chen, X., Jin, L, L. and Qiu, X, M.: Formation and development
596 mechanism of one cyclone over Changjiang-Huaihe River basin and diagnostic
597 analysis of rainstorm. Meteor Mon., 42, 716-723, 2016.
598 DOI: [10.7519/j.issn.1000-0526.2016.06.007](https://doi.org/10.7519/j.issn.1000-0526.2016.06.007)
- 599 Zhang, J, G., Wang, J., Wu, T., Zhou, J, L., Zhong, M., Wang, S, S., Huang, X, Y., Li,
600 S, J., Han, F, R. and Wang, X, C.: Weather system types of extreme precipitation in
601 the middle reaches of the Yangtze River. Torrential Rain and Disasters., 37, 14-23,
602 2018.
603 Doi: [10.3969/j.issn.1004-9045.2018.01.003](https://doi.org/10.3969/j.issn.1004-9045.2018.01.003)
- 604 Zhang, Y, X., Ding, Y, H. and Li, Q, P.: Cyclogenesis Frequency Changes of
605 Extratropical Cyclones in the Northern Hemisphere and East Asia Revealed by
606 ERA40 Reanalysis Data. Meteor Mon., 38, 646-656, 2012.
- 607 Zhou, J, L., Zhang, J, G., Wu, T., Xu, G, Y., Liu, X, W., Wang, J. and Han, F, R.:
608 Characteristics of the mesoscale weather system producing extreme rainstorm in
609 boundary layer during the Meiyu front over the middle reaches of Yangtze River.
610 Meteor Mon., 48, 1007-1019, 2022. DOI: [10.7519/j.issn.1000-0526.2022.052801](https://doi.org/10.7519/j.issn.1000-0526.2022.052801)
- 611 Zhong, Q, M., Ma, J., Wang, L.: Biweekly oscillation of the Meiyu-season precipitation
612 in 2016 and 2020 over the Yangtze Huaihe River basin: A comparative analysis. Acta
613 Meteorologic Sinica., 8, 235-25, 2023. DOI:[10.11676/qxxb2023.20220075](https://doi.org/10.11676/qxxb2023.20220075)
- 614 Zhou, X, M., Zheng, Y, G.: Analysis of Environmental Conditions and Tornado Storm
615 Features of Two Tornadoes in Jiangsu during the Meiyu Period in 2020. Advances in



616 Meteorological Science and Technology., 10, 34-42, 2020.
617 DOI: [10.3969/j.issn.2095-1973.2020.06.008](https://doi.org/10.3969/j.issn.2095-1973.2020.06.008).
618 Zhou, Y., Xia, L.: Statistical Research on Climatic Characteristics of Jianghuai
619 Cyclones. Meteorological and Environmental Sciences., 40, 79-85, 2017.
620 DOI: [10.16765/j.cnki.1673-7148.2017.03.013](https://doi.org/10.16765/j.cnki.1673-7148.2017.03.013)
621 Zhu, M., Lu, H, C. and Yu, Z, H.: Study of Positive Feedback Mechanism for Meso- α
622 Scale Cyclone Growing on Meiyu Front. Chinese Journal of Atmospheric Sciences.,
623 22, 763-770, 1998. Doi: [10.3878/j.issn.1006-9895.1998.05.11](https://doi.org/10.3878/j.issn.1006-9895.1998.05.11)
624